J. Fluid Mech. (2024), *vol*. 998, A55, doi:10.1017/jfm.2024.695

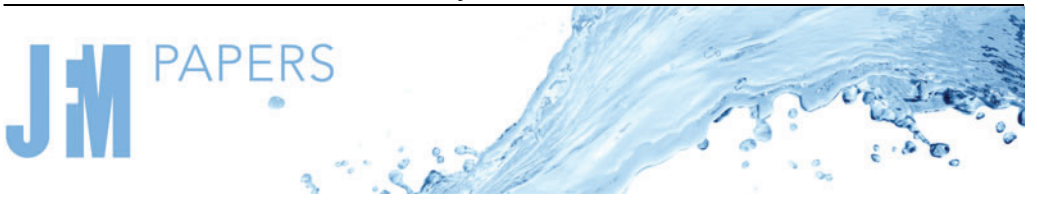

Unifying suspension and granular shear-induced self-diffusion

Shivakumar Athani[1,2], Bloen Metzger[2], Romain Mari[1], Yoël Forterre[2] and Pierre Rognon[3,†]

[1]Univ. Grenoble-Alpes, CNRS, LIPhy, 38000 Grenoble, France

[2]Aix Marseille Univ., CNRS, IUSTI, 13453 Marseille, France

[3]School of Civil Engineering, The University of Sydney, Sydney 2006, NSW, Australia

(Received 3 December 2023; revised 8 April 2024; accepted 17 June 2024)

Shear-induced self-diffusion is a fundamental mode of transport in granular flows. Yet its critical behaviour and dependence on the particle solid fraction are still unclear. Here, we rationalize these dependencies by performing two-dimensional pressure-imposed numerical simulations of dense non-Brownian frictional suspensions. Our results, combined with existing numerical data on inertial granular flows, show that the shear-induced diffusion coefficients of both systems can be captured by a single function of the distance to jamming. They further show that the grain diffusive behaviour is underpinned by a specific random walk process, having a constant elementary step length driven at a frequency that increases with the solid fraction. The proposed scaling laws pave the way for a better understanding of mixing processes in granular media.

Key words: suspensions, dry granular material, granular materials

1. Introduction

Shear-induced self-diffusion describes the random and non-affine particle displacements observed in all flows involving granular materials, be they dry or immersed in a liquid (Eckstein, Bailey & Shapiro 1977; Zik & Stavans 1991; Sierou & Brady 2004). This process is key in many situations in nature and industry as it drives grain mixing and can significantly enhance heat transfers or counterbalance segregation across sheared granular layers (Rognon & Einav 2010; Metzger, Rahli & Yin 2013; Omori *et al.* 2013; Koslover, Chan & Theriot 2017; Thøgersen & Dabrowski 2017; Weijs & Bartolo 2017; Rognon & Macaulay 2021). Yet its description remains incomplete. Widely investigated for low and

† Email address for correspondence: pierre.rognon@sydney.edu.au

moderate solid fractions under volume-imposed conditions (Leighton & Acrivos 1987; Breedveld *et al.* 2002; Leshansky & Brady 2005; Olsson 2010; Vollebregt, Van Der Sman & Boom 2010; Hatano 2011; Metzger *et al.* 2013; Saitoh & Kawasaki 2020, 2022), shear-induced self-diffusion at the continuum scale is described by an effective diffusion coefficient $D = f(\phi)\,\dot{\gamma} d^2$ featuring dependencies on the flow shear rate $\dot{\gamma}$ and the particle diameter d (Leighton & Acrivos 1987). However, the nature and origin of $f(\phi)$, a function of the particle solid fraction ϕ, remain elusive, especially in the dense regime (Vollebregt *et al.* 2010; Artoni *et al.* 2021).

During the past two decades, significant progress has been made in understanding the rheological properties of granular systems using the so-called pressure-imposed approach, where instead of imposing the particle volume fraction, one controls the confining particle stress P (MiDi 2004; Da Cruz *et al.* 2005). The virtue of this approach is to prescribe the normal stress and let the granular layer dilate or compact accordingly. It conveniently allows measurements close to the jamming transition, i.e. when $\phi \to \phi_c$, where ϕ_c is the maximum packing solid fraction. This pressure-imposed approach allowed major progress and in particular the identification of the critical behaviours of the rheological properties of granular flows and dense suspensions (Forterre & Pouliquen 2008; Boyer, Guazzelli & Pouliquen 2011; Guazzelli & Pouliquen 2018). For inertial grains of density ρ, this approach also revealed the scaling relation $D \propto \dot{\gamma} d^2/\sqrt{I}$ between the shear-induced diffusion coefficient D and the inertial number $I = \dot{\gamma} d\sqrt{\rho/P}$, controlling the flow (Kharel & Rognon 2017).

In this paper, we use pressure-imposed simulations to address the behaviour of the shear-induced self-diffusion coefficient in dense suspensions composed of rigid, non-Brownian and frictional particles immersed in a viscous fluid of viscosity η. We first express the shear-induced self-diffusion coefficient D as a function of the viscous number $J = \eta\dot{\gamma}/P$, the analogue of the inertial number for suspensions (Boyer *et al.* 2011; Rognon, Einav & Gay 2011; DeGiuli *et al.* 2015; Guazzelli & Pouliquen 2018). Then, using the dilatancy laws $\phi(J)$ and $\phi(I)$ of both suspensions and inertial granular media, we find that the shear-induced self-diffusion coefficient D of both systems follows a similar scaling relation with the distance to jamming $\phi_c - \phi$, identifying the function $f(\phi) = 0.027(\phi_c - \phi)^{-1/2}$. This result indicates that particle self-diffusion is oblivious to the origin of the dissipation mechanism (viscous damping forces or elastic granular collisions) and is determined primarily by geometrical effects. Moreover, we show that in suspensions and inertial granular media, the scaling for the particle-shear-induced self-diffusion coefficient stems from a specific random walk process, featuring a constant elementary step length driven at a frequency that increases with the solid fraction.

2. Method

Simulations are performed using a discrete element method initially built for volume-imposed simulations (Mari *et al.* 2014), and then further developed to address pressure-imposed configurations (Athani *et al.* 2022). This method solves for the motion of individual, inertialess grains considering frictional, linear elastic contacts and lubrication interactions with neighbouring grains, and an interaction with the imposed external shear flow through a viscous drag. More details about the simulation method can be found in Appendix A.

As shown in figure 1(*a*), the system is composed of a monolayer of hard bidisperse spheres of mean diameter d confined between two walls. Black particles constitute the rigid top and bottom walls built out of frozen particles arranged in a disordered configuration.

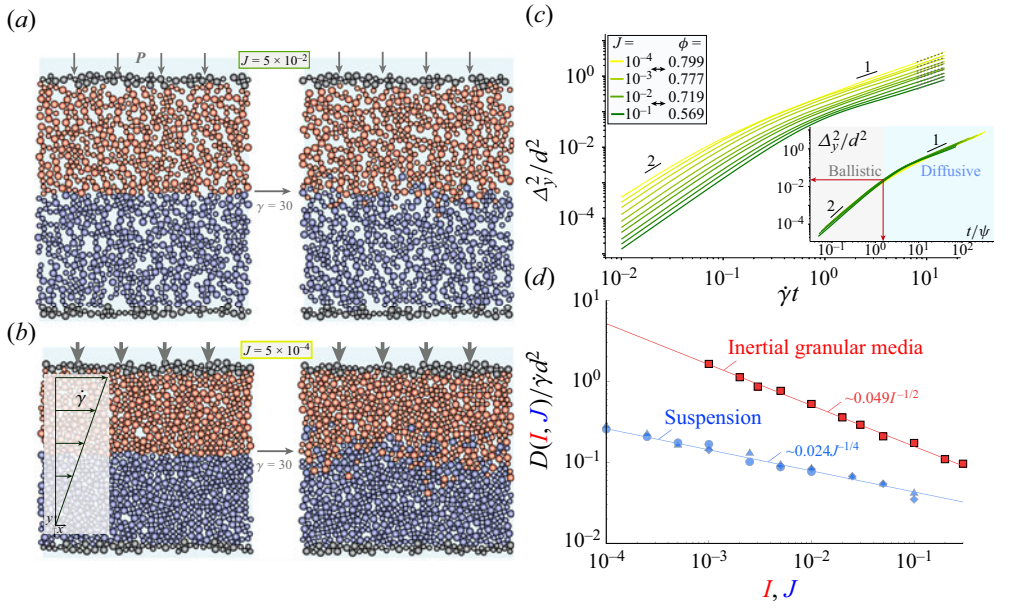

Figure 1. Shear-induced self-diffusion in a two-dimensional suspension and comparison with dry inertial granular media. (*a*,*b*) Snapshots of the suspension shown at strains $\gamma = \dot{\gamma}t = 0$ and 30, sheared under high ($J = 5 \times 10^{-2}$) and low ($J = 5 \times 10^{-4}$) viscous numbers, respectively. Corresponding movies are available online at https://doi.org/10.1017/jfm.2024.695. (*c*) Mean square displacements Δ_y^2/d^2 versus strain $\dot{\gamma}t$ obtained for various imposed steady viscous numbers J. Inset: same data plotted versus t/Ψ, where Ψ is the persistence time. (*d*) Corresponding particle dimensionless diffusion coefficients $D/\dot{\gamma}d^2$ versus J (blue diamonds $\tilde{k} = 10^3$, blue triangles $\tilde{k} = 10^4$, blue circles $\tilde{k} = 10^5$, present study) and comparison with $D/\dot{\gamma}d^2$ versus I for a dry inertial granular system (red squares, data from Macaulay & Rognon 2019). The uncertainty on D arising from fitting the mean square displacement is ± 2 %; typical error bars can be appreciated from the dispersion between runs.

Note that Wang & Brady (2015) developed a pressure imposed code that, by allowing a finite compressibility of the fluid phase, enables us to use Lees–Edwards boundary conditions, thereby preventing the introduction of solid walls. Here, the bottom wall is fixed, while the top wall, permeable to the fluid, moves horizontally to shear the suspension, but is also free to move vertically. The control parameters are the external pressure P acting on the top wall, and the shear rate $\dot{\gamma}$ of the imposed background shear flow. In this pressure-imposed configuration, the solid fraction ϕ is free to adjust owing to the value of the imposed viscous number $J = \eta\dot{\gamma}/P$. Importantly, such a configuration was used previously to simulate the transient migration/dilation of a granular layer under changes of boundary conditions (Athani *et al.* 2022). The present study is focused on the behaviour of the particle shear-induced self-diffusion coefficient when imposing different viscous numbers J. We thus report only measurement performed during steady states, for which the particle pressure and volume fraction are homogeneous across the system. Moreover, this pressure-imposed configuration allows us to perform simulations with a fixed degree of overlap between particle as the parameter $\tilde{k} = k_n/Pd$, where k_n, the particle stiffness, can easily be held constant. Simulations obtained with different values $\tilde{k} = 10^3$, 10^4 and 10^5 show that our results are representative of the rigid grains limit (Da Cruz *et al.* 2005). We take advantage of the pressure-imposed configuration to explore the system in the 'dense' regime, reaching distances to jamming as small

as $\phi_c - \phi = 0.02$, or equivalently, $J = 10^{-4}$. The protocol is as follows. We set the external pressure P and the shear rate $\dot{\gamma}$, then run the simulation until the suspension reaches a steady state (with homogeneous particle pressure and volume fraction profiles), corresponding to the target viscous number $J = \eta\dot{\gamma}/P$. From this point, referred to as $t = 0$, the simulation is performed for 30 additional strain units, over which the particle shear induced self-diffusion coefficient is computed.

3. Results

In figures 1(*a*) and 1(*b*), we illustrate the grain mixing arising from shear-induced diffusion by colour coding the top and bottom particles at $t = 0$. We observe that after 30 strain units, grains have diffused significantly, and that mixing is more pronounced for the lowest viscous number (i.e. for $J = 5 \times 10^{-4}$). To investigate this phenomenology more quantitatively, we measure the particle mean square displacements in the gradient direction $\Delta_y^2(t) = \langle (y_i(t_0 + t) - y_i(t_0))^2 \rangle$, where $y_i(t)$ is the transverse position of grain i at time t, and the operator $\langle \cdot \rangle$ denotes a spatial average including all mobile grains and a temporal average including 10^3 reference times t_0 taken at random during the flow. Figure 1(*c*) shows the normalized mean square displacements Δ_y^2/d^2 versus strain $\dot{\gamma}t$ obtained for different imposed viscous numbers $J \in [10^{-4}, 10^{-1}]$, or equivalent solid fractions $\phi_c - \phi \in [0.02, 0.25]$. After a short ballistic regime, where the mean square displacements increase quadratically with strain, the system transitions towards a linear diffusive regime. The corresponding diffusion coefficients are extracted according to the Einstein formula $D = \lim_{t\to\infty} \Delta_y^2(t)/2t$, by fitting the mean square displacement, using $\Delta_y^2/d^2 = 2(D/\dot{\gamma}d^2)\dot{\gamma}t$, over the strain range highlighted by the dashed lines ($\gamma \in [8, 15]$), where the system has reached its diffusive regime. The resulting shear-induced diffusion coefficients plotted for various values of J in figure 1(*d*) can be well fitted by the simple power law $D(J)/\dot{\gamma}d^2 = 0.024J^{-0.26}$, suggesting that D follows the scaling law

$$\frac{D_{susp}}{\dot{\gamma}d^2} \approx 0.024J^{-1/4}. \tag{3.1}$$

For the sake of clarity, all exponents in the following are similarly rounded to the nearest fractional exponent (within error bars). The fitting procedure, best-fit parameters and associated error bars are provided in Appendix B. The latter scaling law indicates that particles in suspensions tend to diffuse more for smaller values of the viscous number J (or equivalently, for larger ϕ), as previously observed qualitatively in figures 1(*a*) and 1(*b*). Interestingly, Macaulay & Rognon (2019) report a similar scaling law for inertial granular media,

$$\frac{D_{gran}}{\dot{\gamma}d^2} \approx 0.049I^{-1/2}, \tag{3.2}$$

as illustrated in figure 1(*d*). *A priori*, suspensions and inertial granular flows are different systems governed by their own dimensionless numbers, namely J and I, which involve different physical mechanisms. However, as shown in figure 2(*a*), examination of the dilation laws $\phi(J)$ and $\phi(I)$ indicates that for such a frictional suspension,

$$\phi_{susp} \approx \phi_c - 0.64J^{1/2}, \tag{3.3}$$

with $\phi_c = 0.81 \pm 1 \times 10^{-2}$, and for inertial granular media,

$$\phi_{gran} \approx \phi_c - 0.44I, \tag{3.4}$$

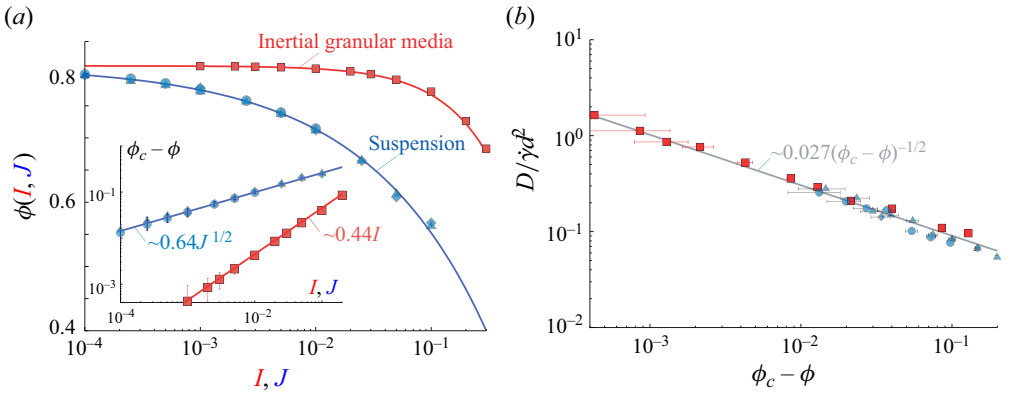

Figure 2. Unifying suspension and granular shear-induced self-diffusion. (*a*) Dilatancy laws $\phi(J)$ for suspensions (blue diamonds $\tilde{k} = 10^3$, blue triangles $\tilde{k} = 10^4$, blue circles $\tilde{k} = 10^5$, present study) and $\phi(I)$ for dry inertial granular media (red squares, data from Da Cruz *et al.* 2005). Inset: same data plotting $\phi_c - \phi$ versus I and J. (*b*) Dimensionless particle diffusion coefficients $D/\dot{\gamma}d^2$ for suspensions and dry inertial granular media versus $\phi_c - \phi$ show a collapse on a single master curve. Uncertainties on ϕ_c are indicated by the horizontal error bars.

with $\phi_c = 0.812 \pm 1 \times 10^{-3}$. By expressing J and I as functions of $\phi_c - \phi$, we expect that the diffusion coefficients of both the suspension, (3.1), and the inertial granular media, (3.2), follow the same scaling law $D_{susp} \sim D_{gran} \sim (\phi_c - \phi)^{-1/2}$. The striking result shown in figure 2(*b*) is that by plotting D_{susp} and D_{gran} versus $\phi_c - \phi$, both sets of data collapse onto a single master curve. More precisely, the diffusion coefficients of suspensions and inertial granular media share not only the same exponent $-1/2$, but also a very similar numerical prefactor, yielding

$$\frac{D_{susp}}{\dot{\gamma}d^2} \approx \frac{D_{gran}}{\dot{\gamma}d^2} \approx 0.027(\phi_c - \phi)^{-1/2}. \tag{3.5}$$

Careful examination of figure 2(*b*) shows that D_{susp} is slightly lower than D_{gran}. (Individual fits of these two data sets are provided in the supplementary material available at https://doi.org/10.1017/jfm.2024.695.) This difference is actually surprisingly small given that the two data sets for suspensions and inertial granular media are obtained from different numerical codes. The near collapse of the data on a single power law indicates that shear-induced diffusion in granular systems is oblivious to the nature of the dissipation mechanism (viscous or inertial), and appears to be mainly geometrical, as set primarily by the particle solid fraction (see § 4 and Appendix D). This is a striking difference compared to other quantities related to dissipation, such as the viscosity or the shear stress, which, owing to stress additivity, collapse only when using a combination of J and I (Trulsson, Andreotti & Claudin 2012; Tapia *et al.* 2022).

To probe the physical origin of the above scaling law, we further analyse the particle trajectories to extract two kinematic quantities: the mean velocity fluctuation $\delta v = \langle v_{y,i}^2 \rangle^{1/2}$ and its persistence time Ψ, which control the particle diffusive behaviour according to $D = \delta v^2 \Psi$ (Rognon & Macaulay 2021). These quantities are obtained following Olsson (2010), DeGiuli *et al.* (2015) and DeGiuli, McElwaine & Wyart (2016) by computing the autocorrelation function of the velocity fluctuations

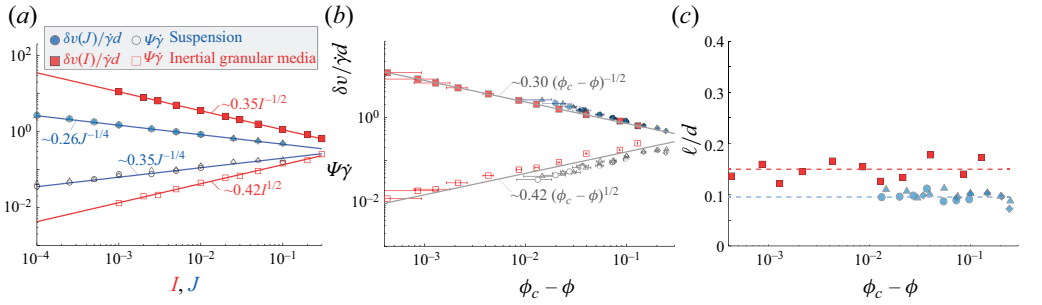

Figure 3. Random walk analysis. (*a*) Normalized velocity fluctuations $\delta v/\dot{\gamma}d$ (filled symbols) and persistence time $\Psi\dot{\gamma}$ (open symbols) versus viscous number J for suspensions (blue symbols, present study), and versus inertial number I for inertial granular media (red symbols, data from Da Cruz *et al.* (2005) for $\delta v(I)$ and from Macaulay & Rognon (2019) for $\Psi(I)$). (*b*) Same data plotted versus $\phi_c - \phi$. (*c*) Same symbols as figure 2.

$C(\tau) = \langle v_{y,i}(t_0)\, v_{y,i}(t_0+\tau)\rangle$. Figure 3(*a*) evidences the scaling laws

$$\frac{\delta v_{susp}}{\dot{\gamma}d} \approx 0.26J^{-1/4} \quad \text{and} \quad \Psi_{susp}\dot{\gamma} \approx 0.35J^{1/4} \tag{3.6a,b}$$

obtained with our analysis for suspensions, and

$$\frac{\delta v_{gran}}{\dot{\gamma}d} \approx 0.35I^{-1/2} \quad \text{and} \quad \Psi_{gran}\dot{\gamma} \approx 0.42I^{1/2} \tag{3.7a,b}$$

for inertial granular media, as reported by Da Cruz *et al.* (2005) for $\delta v(I)$ and by Macaulay & Rognon (2019) for $\Psi(I)$; see also Dumont *et al.* (2023). As before, by virtue of the complementary scalings followed by the dilatancy laws in suspensions and granular media, these data sets are also found to collapse reasonably well when plotted versus $\phi_c - \phi$, yielding the unified scaling laws

$$\frac{\delta v}{\dot{\gamma}d} \approx 0.30(\phi_c-\phi)^{-1/2} \quad \text{and} \quad \Psi\dot{\gamma} \approx 0.42(\phi_c-\phi)^{1/2}, \tag{3.8a,b}$$

shown in figure 3(*b*).

These scaling laws point out the random walk process underpinning the grains' diffusive behaviour: as shown in figure 3(*c*), grains take steps in random directions after a characteristic displacement $\ell = \delta v\Psi$. Individual fits yield $\ell \approx 0.15d$ for inertial grains (red dashed line) and $0.09d$ for suspensions (blue dashed line). Remarkably, the step size ℓ, typically a small fraction of a grain size, is independent of the solid fraction ϕ, and weakly sensitive whether grains are immersed in a viscous fluid or not. By contrast, the step frequency $\Psi^{-1} \sim (\phi_c - \phi)^{-1/2}$ increases when increasing the solid fraction, which is the sole driver of the increase in the normalized diffusivity captured in (3.1). This scenario is further confirmed by the inset of figure 1(*c*), which shows that the mean square displacements collapse onto a single curve $\Delta_y^2(t/\Psi)/d^2$, once time is normalized by the step frequency Ψ^{-1}. For all viscous numbers investigated (or equivalent solid fractions), the transition between ballistic and diffusive regimes occurs at time $t/\Psi \approx O(1)$ and for a typical constant mean square displacement $\Delta_y^2/d^2 \approx 0.02$, close to the square of one elementary step of the random walk $\ell^2/d^2 \approx 0.017$. Note that in the kinetic theory for granular gases, the diffusion coefficient is often plotted as a function of the square root of the granular temperature, equivalent here to the velocity fluctuations δv. As shown in Appendix D, we find that indeed D scales with $\sqrt{T}$, but the data obtained from

suspensions and dry granular media do not collapse onto a single curve. By contrast, the complete dimensional scaling, introducing also either ℓ the step length (such that $D = \delta v \ell$) or equivalently Ψ the persistence time (such that $D = \delta v^2 \Psi$), provides a better match between both data sets.

4. Discussion

The unified framework introduced here allows us to better understand and predict the process of shear-induced self-diffusion in both suspensions and dry inertial granular flows. Results from two-dimensional simulations highlight scaling laws for the diffusivity as a function of the flow property, grain diameter and solid fraction, and provide a physical rationale for its origin in term of a granular random walk. Of fundamental importance is the finding of a unique scaling law for $D \approx 0.027(\phi_c - \phi)^{-1/2}\dot{\gamma} d^2$ that applies for both suspensions and inertial granular media. We also show that this scaling stems from a specific random walk process having a constant elementary step length ℓ/d driven at frequency $\Psi^{-1} \sim \dot{\gamma}(\phi_c - \phi)^{-1/2}$, which increases with the solid fraction.

These results call for several comments. The proposed scaling law for the particle diffusion coefficient diverges at jamming, i.e. when $J \to 0$ or $I \to 0$ (equivalently, when $\phi \to \phi_c$). As it is unlikely that particles can experience an infinite displacement over a small but finite strain, we anticipate that this scaling should ultimately break down and saturate when $\phi \to \phi_c$. For a finite-size system, a saturation of the particle diffusion coefficient is expected when correlated structures in the flow start to reach the system size, as observed with granular flows in Kharel & Rognon (2017).

Some caution is also required as the scaling laws presented here were obtained in a uniform shear flow (other non-uniform flows could lead to different scaling relations). These scaling laws were also drawn from two-dimensional numerical simulations, although previous numerical works show that exponents characterizing the divergence of macroscopic quantities are unchanged for simulations performed in two and three dimensions (DeGiuli *et al.* 2015).

An important remaining question is the role played by particle friction. Simulations here were performed with a particle friction coefficient $\mu_p = 0.5$. However, other studies have shown that changes in the particle friction coefficient can affect scaling exponents of velocity fluctuations and persistence time (Trulsson, DeGiuli & Wyart 2017). Whether these changes can alter the unified description put forth in the present study still needs to be determined. For instance, the scaling analysis proposed in Olsson (2010) for frictionless particles suggests that in this case, $D \sim (\phi_c - \phi)^{-0.8}$. (Olsson (2010) identified that the particle diffusion coefficient for frictionless particles in the hard core limit obeys the scaling function $D/\dot{\gamma}^q \sim (\delta\phi/\dot{\gamma}^{1/(\beta+\Delta)})^{-x}$, where $\delta\phi = \phi - \phi_c$. Using that $D \sim \dot{\gamma}$, one expects $D \sim \delta\phi^{-0.8}$ as x must be equal to $(1-q)(\beta+\Delta)$, with $q \approx 0.78$ and $1/(\beta+\Delta) \approx 0.275$.)

Our analysis differs from the recent approaches to unify rheological flow rules of suspensions and inertial granular media using the dimensionless viscous-inertial number $K = J + \alpha I^2$ (Trulsson *et al.* 2012; Ness & Sun 2015; Tapia *et al.* 2022). The viscous-inertial number is built from the idea of stress additivity, and gives the adjustable dimensionless prefactor α an important role since it allows us to accommodate the difference in magnitude of the dissipation mechanisms at play in suspensions and granular media. Stress additivity seems to be well verified (Trulsson *et al.* 2012; Ness & Sun 2015; Tapia *et al.* 2022) – although not always (Otsuki & Hayakawa 2009; Vågberg, Olsson & Teitel 2016; Ness, Seto & Mari 2022) – thereby yielding a good collapse of

quantities involving dissipation, like the effective friction or the shear stress. However, unlike the inertial number I for inertial granular media and the viscous number J for viscous suspensions, the viscous-inertial number is not a direct outcome of dimensional analysis. There is therefore no reason to expect that all observables are functions of K. It particular, we do not expect that stress additivity has any relevance for a microscopic transport quantity such as D, and therefore that D is a function of K. That a good collapse is readily found by plotting D versus $(\phi_c - \phi)^{-1/2}$ rather shows that self-diffusion is primarily set by steric, geometrical effects, and is oblivious to the dissipation mechanism. The idea that transport properties in granular media are purely kinematic, while stresses depend on the nature of the interactions, was also put forth in Maiti & Heussinger (2014). Nonetheless, if we further assume stress additivity, then $(\phi_c - \phi)$ is itself a function of K, and we therefore expect to be able to collapse our diffusion coefficient data with K. As shown in Appendix C, we can indeed carefully adjust the value of α to find a good collapse for both suspensions and granular media, which we interpret as merely a validation of the hypothesis of stress additivity. Finally, note that the behaviour of the collective shear-induced diffusion coefficient, which drives particle migration in inhomogeneous systems, is expected to be different. The latter quantity describes the response of the system to particles stress gradient (osmotic compressibility; Leshansky & Brady 2005), and should therefore depend on the nature of the dissipation mechanism. Nonetheless, establishing the link between self and collective diffusivities in the dense regime would be an interesting problem to investigate in future studies.

To conclude, we can draw some interesting perspectives on mixing granular and suspension flows, which represents a considerable challenge in industry. For such athermal systems, particle diffusion is a self-induced process prescribed by the flow itself, as opposed to standard mixing problems where advection and molecular diffusion are independent. Having $D \sim f(\phi)\,\dot{\gamma} d^2$ from (3.5), one obtains a Péclet number $Pe \sim \dot{\gamma} d^2/D \sim 1/f(\phi)$, which characterizes the mixing process, that is independent of the shear rate (under volume-imposed conditions) (Souzy *et al.* 2018; Villermaux 2019). Mixing dense granular media must then in essence be a purely kinematic process: the state of the mixture should depend not on the rate at which the substrate is deformed, only on the magnitude of the deformation – an interesting and quite relevant problem that certainly deserves further investigations.

Supplementary material. Supplementary material is available at https://doi.org/10.1017/jfm.2024.695.

Acknowledgements. We thank O. Pouliquen, M. Wyart and E. Villermaux for discussions.

Funding. This work was supported by ANR ScienceFriction (ANR-18-CE30-0024), and ARC Wear (DP200101927).

Declaration of interests. The authors report no conflict of interest.

Author ORCIDs.
Bloen Metzger https://orcid.org/0000-0003-3031-6543;
Romain Mari https://orcid.org/0000-0001-7877-416X;
Yoël Forterre https://orcid.org/0000-0001-6052-7291;
Pierre Rognon https://orcid.org/0000-0001-7071-2247.

Appendix A. Simulating plane shear of dense suspensions

The material is a suspension of non-Brownian grains in a fluid of viscosity η in the Stokes regime. The system is quasi-two-dimensional to avoid prohibitive simulation times, and

comprises N spherical grains set on the xy plane, using a bidisperse size distribution with diameters d and $1.4d$, mixed in equal volume. The mass of the grains is set to zero to clear inertia and focus on an over-damped dynamics. The equations of motion are obtained by imposing force and torque balances on each particle. Force balance on particle i is $\boldsymbol{f}_{d,i} + \boldsymbol{f}_{l,i} + \boldsymbol{f}_{c,i} = 0$. Here, we omit torque balance, which involves the same interactions (Mari *et al.* 2014). In the latter equation, $\boldsymbol{f}_{d,i} = -3\pi\eta d_i(\boldsymbol{v_i} - \boldsymbol{v}_\infty(y_i))$ is the Stokes drag, with r_i the radius of the particle i, $\boldsymbol{v}_i$ its velocity, and $\boldsymbol{v}_\infty(y_i) = (\dot{\gamma} y_i, 0)$ the assumed background fluid velocity. The force $\boldsymbol{f}_{l,i}$ is the resulting force of all pairwise lubrication interactions involving particle i. We include the dominant modes of lubrication (the 'squeeze', 'shear' and 'pump' modes; Ball & Melrose 1997). These provide normal and tangential forces which magnitude depend on the dimensionless gap between particles i and j located at positions $\boldsymbol{r}_i$ and $\boldsymbol{r}_j$, $h_{ij} = 4|\boldsymbol{r}_j - \boldsymbol{r}_i|/(d_i + d_j) - 2$, as $1/(h_{ij} + \delta)$ and $\log(h_{ij} + \delta)$, respectively. The regularization length $\delta = 10^{-2}$ mimics the presence of particle roughness on this scale that allows for contact to happen despite lubrication. The force $\boldsymbol{f}_{c,i}$ is the resulting contact force on i. Contact forces involve normal and frictional tangential components, both modelled with spring and dashpot (Cundall & Strack 1979). Contacts follow Coulomb's law with a friction coefficient 0.5. The ratio of tangential to normal stiffnesses is set as $k_t/k_n = 0.5$, and the dashpot resistances are set to match the normal and tangential resistance of lubrication right at contact (i.e. for $h_{ij} = 0$). The normal stiffness is varied as $k_n \in [10^3, 10^5]Pd$ to show that our results are representative of the hard particle limit. The full detail of the interactions and numerical scheme are presented in Mari *et al.* (2014).

The suspension is sheared between two rough boundaries, which simultaneously prescribe a constant shear rate $\dot{\gamma}$ and a constant normal stress P. Both boundaries are made of grains similar to the flowing grains, but moving as a rigid body: grains forming a boundary share the same velocity in the x and y directions, and have no rotation. To prescribe the shear rate, one boundary is kept fixed and the other moves along the x direction at speed $V(t) = \dot{\gamma}H(t)$, where H is the mean distance between the two boundaries. The system is periodic in the x direction. To keep the normal stress P constant, the moving boundary can also move in the y direction. Again using linearity of dashpot and lubrication forces in velocities, the y velocity component is set at every time step so that the sum of all contact and hydrodynamic forces that particles in the moving wall exert on the particles in the suspension is PL_x, with L_x the wall length (Athani *et al.* 2022). The motion along y of the wall implies dilation or contraction of the sheared material. We checked that the steady flow solid fraction ϕ is independent on the initial solid fraction ϕ_i, ruling out potential micro-structural memory effect. The results were obtained with a system comprised of $N = 1000$ grains. We checked that systems comprised of $N = 500$ and 1500 yielded similar diffusivity, velocity fluctuations and time persistence.

Appendix B. Fitting procedure, parameters and uncertainty

Equations (3.1), (3.2), (3.5)–(3.8) are obtained by fitting the numerical data using a power law of the form $g(x) = ax^b$ and by letting both a and b be free parameters. Fits are performed in the log-log space, effectively fitting the log of the quantities $\log(g(\log(x)))$ by an affine function $\log(a) + \log(b)\,x$. For the sake of clarity, the best-fit exponents b were rounded to the nearest fractional exponent (within their respective standard error). Table 1 summarizes the values of the best-fit parameters and their respective standard errors.

The dilatancy laws (3.3) and (3.4) were fitted by a function $\phi(x) = \phi_c - ax^b$. First, the value of ϕ_c is obtained by adjusting ϕ_c until the data for $\phi - \phi_c$ best align along a

$g(x)$	x	a	b	System	Figure
$D/\dot{\gamma}d^2$	J	0.024 ± 0.002	-0.26 ± 0.02	Susp.	Figure 1(d)
$D/\dot{\gamma}d^2$	I	0.049 ± 0.008	-0.51 ± 0.02	Gran.	Figure 1(d)
$D/\dot{\gamma}d^2$	$\phi_c - \phi$	0.019 ± 0.006	-0.61 ± 0.1	Susp.	Figure 2(b)
$D/\dot{\gamma}d^2$	$\phi_c - \phi$	0.032 ± 0.006	-0.50 ± 0.06	Gran.	Figure 2(b)
$D/\dot{\gamma}d^2$	$\phi_c - \phi$	0.027 ± 0.002	-0.53 ± 0.08	Both	Figure 2(b)
$\delta v/\dot{\gamma}d$	J	0.258 ± 0.008	-0.25 ± 0.04	Susp.	Figure 3(a)
$\delta v/\dot{\gamma}d$	I	0.355 ± 0.008	-0.498 ± 0.002	Gran.	Figure 3(a)
$\delta v/\dot{\gamma}d$	$\phi_c - \phi$	0.25 ± 0.01	-0.54 ± 0.07	Susp.	Figure 3(b)
$\delta v/\dot{\gamma}d$	$\phi_c - \phi$	0.21 ± 0.01	-0.48 ± 0.05	Gran.	Figure 3(b)
$\delta v/\dot{\gamma}d$	$\phi_c - \phi$	0.30 ± 0.02	-0.46 ± 0.06	Both	Figure 3(b)
$\Psi\dot{\gamma}$	J	0.35 ± 0.02	0.24 ± 0.02	Susp.	Figure 3(a)
$\Psi\dot{\gamma}$	I	0.42 ± 0.04	0.52 ± 0.04	Gran.	Figure 3(a)
$\Psi\dot{\gamma}$	$\phi_c - \phi$	0.37 ± 0.06	0.51 ± 0.06	Susp.	Figure 3(b)
$\Psi\dot{\gamma}$	$\phi_c - \phi$	0.60 ± 0.05	0.50 ± 0.04	Gran.	Figure 3(b)
$\Psi\dot{\gamma}$	$\phi_c - \phi$	0.42 ± 0.05	0.50 ± 0.05	Both	Figure 3(b)

Table 1. Best fit parameters and errors bars obtained when fitting (3.1), (3.2), (3.5)–(3.8) by $g(x) = ax^b$.

$\phi(x)$	x	ϕ_c	a	b	System	Figure
ϕ	J	0.81 ± 0.01	0.64 ± 0.02	0.42 ± 0.01	Susp.	Figure 2(a)
ϕ	I	0.812 ± 0.001	0.44 ± 0.02	1.02 ± 0.01	Gran.	Figure 2(a)

Table 2. Best fit parameters and errors bars obtained when fitting (3.3) and (3.4) by $\phi(x) = \phi_c - ax^b$.

straight line in log-log scales. Then ϕ_c is fixed, $\phi - \phi_c$ is fitted by the power law ax^b by letting both a and b be free parameters. Finally, the error on ϕ_c is estimated by fitting again $\phi(x) = \phi_c - ax^b$ by letting ϕ_c be a free parameter but fixing a and b. The difference between the initially estimated value of ϕ_c and that returned by this last fit provides an estimate of the error on ϕ_c. The error bar on ϕ_c is represented in figures 2(b) and 3(b). Table 2 summarizes the values of the best-fit parameters and their respective standard errors.

Appendix C. Unifying suspension and granular self-diffusion using $K = J + \alpha I^2$

In the spirit of Trulsson *et al.* (2012) and Tapia *et al.* (2022), figures 4(a) and 4(b) revisit the data shown in figures 1(d) and 3(a). Here, self-diffusion coefficients, velocity fluctuations and persistence times are plotted versus the dimensionless number $K = J + \alpha I^2$, where α is a numerical fitting factor. Here too, shear-induced self-diffusion coefficients from suspension and inertial granular media are found to collapse on a single curve $D/\dot{\gamma}d^2 = 0.027K^{-1/4}$, with $\alpha = 0.025$. Similarly, the normalized velocity fluctuations follow $\delta v/\dot{\gamma}d^2 = 0.25K^{-1/4}$ and persistence time $\Psi\dot{\gamma} = 0.44K^{1/4}$, with $\alpha = 0.4$.

Appendix D. Scaling of D with the granular temperature

In line with the picture of a random walk, the diffusion coefficient should follow $D = \delta v^2 \Psi = \delta v \ell$, where $\delta v = \sqrt{T}$ are the velocity fluctuations, by definition equal to the

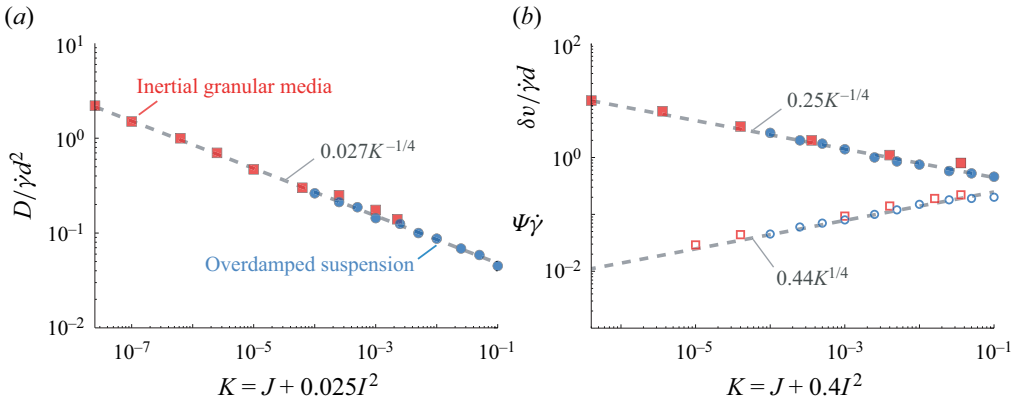

Figure 4. Unifying suspension and granular shear-induced self-diffusion using $K = J + \alpha I^2$. (*a*) Normalized shear-induced self-diffusion coefficients from figure 1(*d*) plotted versus $K = J + 0.025I^2$. (*b*) Normalized velocity fluctuations $\delta v/\dot{\gamma}d$ (filled symbols) and persistence times $\Psi\dot{\gamma}$ (open symbols) from figure 3(*a*) plotted versus $K = J + 0.4I^2$.

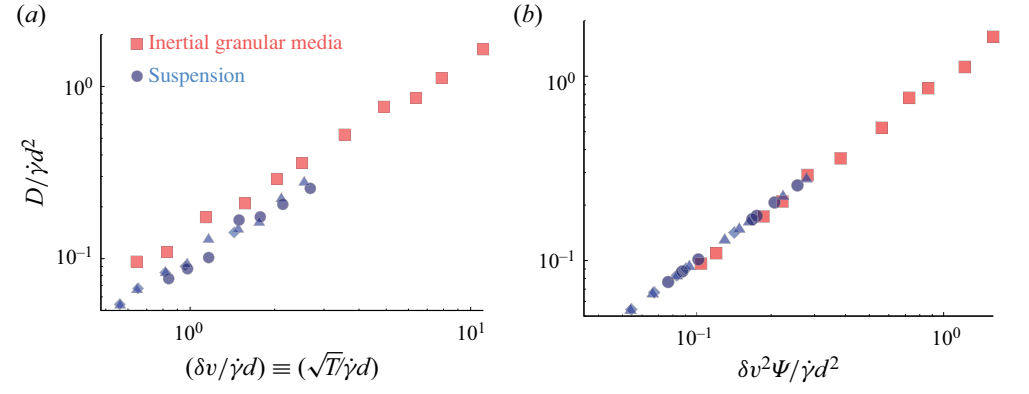

Figure 5. Diffusion coefficient and granular temperature. (*a*) Normalized shear induced self-diffusion coefficient $D/\dot{\gamma}d^2$ versus square root of the granular temperature $\sqrt{T}/\dot{\gamma}d = \delta v/\dot{\gamma}d$. (*b*) Same data versus $\delta v^2\Psi/\dot{\gamma}d^2 \equiv \delta v\ell/\dot{\gamma}d^2$.

square root of the granular temperature (in the kinetic theory of granular gases, e.g. Artoni *et al.* 2021), Ψ is the persistence time, and $\ell = \delta v\Psi$ is the step length. As a result, we find that D scales with $\sqrt{T} = \delta v$, but the data obtained from suspensions and dry granular media do not collapse onto a single curve; see figure 5(*a*). By contrast, plotting D versus $\delta v\ell = \delta v^2\Psi$, which accounts for the difference in ℓ (or Ψ) in suspensions and inertial granular media, provides a full collapse of the data, see figure 5(*b*). These results show that the description of the shear induced self-diffusion coefficient cannot be unified solely using the square root of the granular temperature, one must account for the full dimensional scaling, introducing also either ℓ the step length (such that $D = \delta v\ell$) or equivalently Ψ the persistence time (such that $D = \delta v^2\Psi$).

References

Artoni, R, Larcher, M., Jenkins, J.T. & Richard, P. 2021 Self-diffusion scalings in dense granular flows. *Soft Matt.* **17** (9), 2596–2602.

ATHANI, S., METZGER, B., FORTERRE, Y. & MARI, R. 2022 Transient flows and migration in granular suspensions: key role of Reynolds-like dilatancy. *J. Fluid Mech.* **949**, A9.

BALL, R.C. & MELROSE, J.R. 1997 A simulation technique for many spheres in quasi-static motion under frame-invariant pair drag and Brownian forces. *Physica* A **247** (1–4), 444–472.

BOYER, F., GUAZZELLI, É. & POULIQUEN, O. 2011 Unifying suspension and granular rheology. *Phys. Rev. Lett.* **107** (18), 188301.

BREEDVELD, V., VAN DEN ENDE, D., BOSSCHER, M., JONGSCHAAP, R.J.J. & MELLEMA, J. 2002 Measurement of the full shear-induced self-diffusion tensor of noncolloidal suspensions. *J. Chem. Phys.* **116** (23), 10529–10535.

CUNDALL, P.A. & STRACK, O.D.L. 1979 A discrete numerical model for granular assemblies. *Géotechnique* **29** (1), 47–65.

DA CRUZ, F., EMAM, S., PROCHNOW, M., ROUX, J.-N. & CHEVOIR, F. 2005 Rheophysics of dense granular materials: discrete simulation of plane shear flows. *Phys. Rev.* E **72** (2), 021309.

DEGIULI, E., DÜRING, G., LERNER, E. & WYART, M. 2015 Unified theory of inertial granular flows and non-Brownian suspensions. *Phys. Rev.* E **91** (6), 062206.

DEGIULI, E., MCELWAINE, J.N. & WYART, M. 2016 Phase diagram for inertial granular flows. *Phys. Rev.* E **94** (1), 012904.

DUMONT, D., BONNEAU, H., SALEZ, T., RAPHAEL, E. & DAMMAN, P. 2023 Microscopic foundation of the $\mu(I)$ rheology for dense granular flows on inclined planes. *Phys. Rev. Res.* **5** (1), 013089.

ECKSTEIN, E.C., BAILEY, D.G. & SHAPIRO, A.H. 1977 Self-diffusion of particles in shear flow of a suspension. *J. Fluid Mech.* **79** (1), 191–208.

FORTERRE, Y. & POULIQUEN, O. 2008 Flows of dense granular media. *Annu. Rev. Fluid Mech.* **40**, 1–24.

GDR MIDI 2004 On dense granular flows. *Eur. Phys. J.* E **14** (4), 341–365.

GUAZZELLI, É. & POULIQUEN, O. 2018 Rheology of dense granular suspensions. *J. Fluid Mech.* **852**, P1.

HATANO, T. 2011 Rheology and dynamical heterogeneity in frictionless beads at jamming density. *J. Phys.: Conf. Ser.* **319**, 012011.

KHAREL, P. & ROGNON, P. 2017 Vortices enhance diffusion in dense granular flows. *Phys. Rev. Lett.* **119** (17), 178001.

KOSLOVER, E.F., CHAN, C.K. & THERIOT, J.A. 2017 Cytoplasmic flow and mixing due to deformation of motile cells. *Biophys. J.* **113** (9), 2077–2087.

LEIGHTON, D. & ACRIVOS, A. 1987 Measurement of shear-induced self-diffusion in concentrated suspensions of spheres. *J. Fluid Mech.* **177**, 109–131.

LESHANSKY, A.M. & BRADY, J.F. 2005 Dynamic structure factor study of diffusion in strongly sheared suspensions. *J. Fluid Mech.* **527**, 141–169.

MACAULAY, M. & ROGNON, P. 2019 Shear-induced diffusion in cohesive granular flows: effect of enduring clusters. *J. Fluid Mech.* **858**, R2.

MAITI, M. & HEUSSINGER, C. 2014 Rheology near jamming: the influence of lubrication forces. *Phys. Rev.* E **89** (5), 052308.

MARI, R., SETO, R., MORRIS, J.F. & DENN, M.M. 2014 Shear thickening, frictionless and frictional rheologies in non-Brownian suspensions. *J. Rheol.* **58** (6), 1693–1724.

METZGER, B., RAHLI, O. & YIN, X. 2013 Heat transfer across sheared suspensions: role of the shear-induced diffusion. *J. Fluid Mech.* **724**, 527–552.

NESS, C., SETO, R. & MARI, R. 2022 The physics of dense suspensions. *Annu. Rev. Condens. Matter Phys.* **13** (1), 97–117.

NESS, C. & SUN, J. 2015 Flow regime transitions in dense non-Brownian suspensions: rheology, microstructural characterization, and constitutive modeling. *Phys. Rev.* E **91** (1), 012201.

OLSSON, P. 2010 Diffusion and velocity autocorrelation at the jamming transition. *Phys. Rev.* E **81** (4), 040301.

OMORI, T., ISHIKAWA, T., IMAI, Y. & YAMAGUCHI, T. 2013 Shear-induced diffusion of red blood cells in a semi-dilute suspension. *J. Fluid Mech.* **724**, 154–174.

OTSUKI, M. & HAYAKAWA, H. 2009 Universal scaling for the jamming transition. *Prog. Theor. Phys.* **121** (3), 647–655.

ROGNON, P. & EINAV, I. 2010 Thermal transients and convective particle motion in dense granular materials. *Phys. Rev. Lett.* **105** (21), 218301.

ROGNON, P., EINAV, I. & GAY, C. 2011 Flowing resistance and dilatancy of dense suspensions: lubrication and repulsion. *J. Fluid Mech.* **689**, 75–96.

ROGNON, P. & MACAULAY, M. 2021 Shear-induced diffusion in dense granular fluids. *Soft Matt.* **17** (21), 5271–5277.

SAITOH, K. & KAWASAKI, T. 2020 Critical scaling of diffusion coefficients and size of rigid clusters of soft athermal particles under shear. *Front. Phys.* **8**, 99.

SAITOH, K. & KAWASAKI, T. 2022 Shear-induced diffusion and dynamic heterogeneities in dense granular flows. *Front. Phys.* **10**, 988.

SIEROU, A. & BRADY, J.F. 2004 Shear-induced self-diffusion in non-colloidal suspensions. *J. Fluid Mech.* **506**, 285–314.

SOUZY, M., ZAIER, I., LHUISSIER, H., LE BORGNE, T. & METZGER, B. 2018 Mixing lamellae in a shear flow. *J. Fluid Mech.* **838**, R3.

TAPIA, F., ICHIHARA, M., POULIQUEN, O. & GUAZZELLI, É. 2022 Viscous to inertial transition in dense granular suspension. *Phys. Rev. Lett.* **129** (7), 078001.

THØGERSEN, K. & DABROWSKI, M. 2017 Mixing of the fluid phase in slowly sheared particle suspensions of cylinders. *J. Fluid Mech.* **818**, 807–837.

TRULSSON, M., ANDREOTTI, B. & CLAUDIN, P. 2012 Transition from the viscous to inertial regime in dense suspensions. *Phys. Rev. Lett.* **109** (11), 118305.

TRULSSON, M., DEGIULI, E. & WYART, M. 2017 Effect of friction on dense suspension flows of hard particles. *Phys. Rev.* E **95** (1), 012605.

VÅGBERG, D., OLSSON, P. & TEITEL, S. 2016 Critical scaling of Bagnold rheology at the jamming transition of frictionless two-dimensional disks. *Phys. Rev.* E **93** (5), 052902.

VILLERMAUX, E. 2019 Mixing versus stirring. *Annu. Rev. Fluid Mech.* **51**, 245–273.

VOLLEBREGT, H.M., VAN DER SMAN, R.G.M. & BOOM, R.M. 2010 Suspension flow modelling in particle migration and microfiltration. *Soft Matt.* **6** (24), 6052–6064.

WANG, M. & BRADY, J.F. 2015 Constant stress and pressure rheology of colloidal suspensions. *Phys. Rev. Lett.* **115** (15), 158301.

WEIJS, J.H. & BARTOLO, D. 2017 Mixing by unstirring: hyperuniform dispersion of interacting particles upon chaotic advection. *Phys. Rev. Lett.* **119** (4), 048002.

ZIK, O. & STAVANS, J. 1991 Self-diffusion in granular flows. *Europhys. Lett.* **16** (3), 255.